ELSEVIER

Colloids and Surfaces A: Physicochem. Eng. Aspects 226 (2003) 101–118

COLLOIDS AND SURFACES A

www.elsevier.com/locate/colsurfa

Analytical solutions for monodisperse and polydisperse colloid transport in uniform fractures

Scott C. James [a,*], Constantinos V. Chrysikopoulos [b]

[a] *Sandia National Laboratories, Geohydrology Department, P.O. Box 5800, Albuquerque, NM 87185 0735, USA*
[b] *Civil and Environmental Engineering Department, University of California, Irvine, CA 92697 2175, USA*

Received 14 January 2003; received in revised form 29 May 2003; accepted 10 June 2003

Abstract

Analytical solutions are derived describing the transport of suspensions of monodisperse as well as polydisperse colloid plumes of neutral buoyancy within a fracture with uniform aperture. Various initial and boundary conditions are considered. It is shown that both the finite colloid size and the characteristics of the colloid diameter distribution significantly affect the shape of colloid concentration breakthrough curves. Furthermore, increasing the standard deviation of the colloid diameter enhances colloid spreading and increases the number of attached colloids when colloid–wall interactions are taken into account. Excellent agreement between available experimental data and the analytical solution for the case of an instantaneous release of monodisperse colloids in a natural fracture is observed.

Keywords: Analytical solutions; Uniform fracture; Monodisperse colloids; Polydisperse colloids; Effective parameters; Filtration

1. Introduction

Characterization of colloid and reactive contaminant fate and transport in fractured subsurface formations is the focus of many recent studies [1–6]. These studies suggest that knowledge of the coupled hydrodynamic flow, contaminant transport, and surface reaction processes taking place in a single fracture are fundamental to improving our understanding of reactive contaminant transport in fractured subsurface formations. Both field and laboratory studies indicate that contaminants can migrate while sorbed on the surface of colloids [7–10]. Consequently, colloids affect the mobility of soluble contaminants in fractures as the sorbed contaminants assume the transport characteristics of the colloids that may be significantly different from their own.

Colloids are present in the subsurface in the form of metal oxides, humic macromolecules, bacteria, and viruses [11]. In fractured media, colloids are often formed by microerosion of minerals present in the solid matrix because of formation crushing in association with tectonic activity [12]. When contaminants are released into a subsurface formation of fractured clay or rock, the fractures can provide preferential pathways for colloid migration. Because

* Corresponding author.
E-mail addresses: scjames@sandia.gov (S.C. James), costas@eng.uci.edu (C.V. Chrysikopoulos).

0927-7757/$ – see front matter © 2003 Elsevier B.V. All rights reserved.
doi:10.1016/S0927-7757(03)00316-9

release of colloids in an aquifer can be sudden (e.g., disruptive events like earthquakes) or continuous (e.g., degradation of vitrified waste), both instantaneous and constant concentration boundary conditions should be investigated. Furthermore, most of the studies published in the literature focus on monodisperse colloid transport. However, colloid plumes are rarely composed of a single species, necessitating the study of polydisperse distributions. In addition, because colloid interactions with the solid matrix significantly affect their transport [13], both reversible and irreversible attachment (often termed filtration or sorption) of colloids with the medium should be considered.

Taylor [14] introduced an effective dispersion coefficient for soluble matter flowing in a cylindrical tube (the Taylor dispersion coefficient), which is a function of the dissolved constituent's molecular diffusion coefficient and the fundamental system parameters (i.e., centerline flow velocity and tube radius). Aris [15] extended this pioneering work by employing moment analysis to obtain results in a more generalized manner. These original studies, however, apply only to non-reactive solute transport. Sankarasubramanian and Gill [16] and Brenner [17,18] continued the study of internal flow and transport by developing exact solutions for the dispersion of reactive solutes in a tube. Following the Taylor–Aris procedures, scientists have examined various aspects of contaminant transport in parallel-plate geometries. DeGance and Johns [19] and Shapiro and Brenner [20–22] have obtained approximate analytical models for the dispersion of reactive solutes in cylindrical or parallel-plate geometries and concluded that the Taylor dispersion coefficient needs to be modified to account for solute flux at the system boundaries due to solute reactions with the walls. There are several examples of analytical solutions for contaminant transport in fractured porous media where contaminants are subject to plug flow advection, dispersion, matrix diffusion, surface and matrix sorption, and decay [23–25]. Abdel-Salam and Chrysikopoulos [26] derived closed form analytical solutions for colloid transport in single uniform, porous fractures with and without colloid penetration into the rock matrix for constant concentration as well as constant flux boundary conditions. It was shown that axial advection, transverse diffusion, and penetration into or reaction with the solid matrix govern colloid migration in fractures.

It is often assumed in studies of transport in porous media that particles are infinitesimally small; however, it has been shown that the finite size of colloids also affects their transport properties [27]. Polydisperse colloid transport in water saturated, uniform and variable aperture fractures has been numerically simulated by particle tracking schemes [28–30]. It was observed that the smallest colloids of a plume preferentially attach onto the fracture walls, whereas the largest colloids are transported faster and further through the fracture. It was also shown that a distribution of colloid diameters increases plume spreading (elongated breakthrough curves).

The governing partial differential equations for transport in a fracture are linear with respect to the dependent variable (i.e., colloid concentration). Therefore, analytical solutions to polydisperse colloid transport in a fracture can be derived from corresponding analytical solutions to monodisperse colloid transport through use of the superposition principle. In the present study, two sets of boundary conditions are considered: instantaneous injection and a constant concentration inlet boundary condition. Initially, there are no colloids in the fractures. Solutions are developed subject to both inlet boundary conditions without filtration as well as when colloids irreversibly and reversibly attach onto the fracture walls. It should be noted that the analytical solutions presented in this work are applicable to any distribution of colloid sizes, but model simulations are presented here for one monodisperse and three log-normal polydisperse distributions.

2. Development of models

2.1. Governing transport equations

Consider the miscible displacement of a fluid initially free of colloids by another fluid containing hard colloids of neutral buoyancy within a fracture formed by two semi infinite, non-porous, parallel plates of unit depth as shown in Fig. 1. The governing equations for colloid transport in this fracture account for advection, diffusion, and colloid accumulation at the fracture walls and are

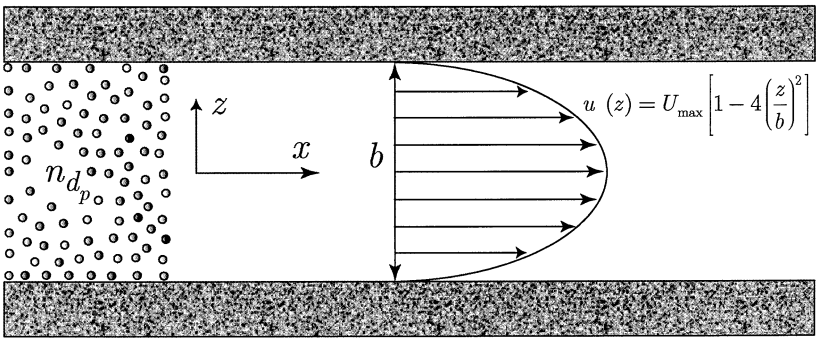

Fig. 1. Schematic illustration of the fracture considered in this study.

given by:

$$\frac{\partial n_{d_p}(x,\ z,\ t)}{\partial t} = \mathcal{D}_{d_p}\left[\frac{\partial^2 n_{d_p}(x,\ z,\ t)}{\partial x^2} + \frac{\partial^2 n_{d_p}(x,\ z,\ t)}{\partial z^2}\right] - u(z)\frac{\partial n_{d_p}(x,\ z,\ t)}{\partial x}, \quad (1)$$

$$\frac{\partial n^*_{d_p}}{\partial t} = \mp\, \mathcal{D}_{d_p}\frac{\partial n_{d_p}(x,\ \pm b/2,\ t)}{\partial z}, \quad (2)$$

where n_{d_p} is the temporally and spatially varying number density (concentration) of colloids with diameter d_p; $n^*_{d_p}$ is the time and space dependent number of attached colloids per unit surface area of the fracture wall; $\mathcal{D}_{d_p}$ is the molecular diffusion coefficient of a colloid with diameter d_p; $u(z)$ is the local interstitial fluid velocity; x is the coordinate in the axial or flow direction; and z is the coordinate perpendicular to the walls of the fracture with its origin at the center of the fracture. The $\mp$ sign in Eq. (2) accounts for the rate of change in colloid concentration due to diffusive flux at $z = \pm b/2$. It is assumed that a fully developed Poiseuille velocity distribution exists within the fracture defined by [31] (p. 392).

$$u(z) = U_{\max}\left[1 - 4\left(\frac{z}{b}\right)^2\right], \quad (3)$$

with mean fluid velocity $2U_{\max}/3$; where $U_{\max}$ is the maximum, or centerline, velocity of the interstitial fluid; and b is the aperture of the fracture. Although colloid concentrations greater than 20% by volume tend to blunt the parabolic velocity [32,33], it is assumed here that colloid concentrations do not affect the velocity. The molecular diffusion coefficient of a spherical particle in the absence of interaction with other colloids is given by the Stokes–Einstein diffusion equation [34] (p. 513):

$$\mathcal{D}_{d_p} = \frac{kT}{3\pi\eta d_p}, \quad (4)$$

where k is Boltzmann's constant; T is the absolute temperature and η is the dynamic viscosity of the interstitial fluid. Furthermore, it is assumed that the fluid density and dynamic viscosity are constant and that gravitational effects are negligible. For low ionic strength suspending fluids (<0.1 M), it has been shown that coagulation is minimal, therefore particle–particle interactions are neglected [35]. It should be noted that hydrodynamic, gravitational, van der Waals, and electrostatic forces are not included in the calculation of colloid velocity and colloids are not allowed to penetrate the fracture walls. The coupled differential Eqs. (1) and (2) take into account the relationship between suspended colloids within the fracture and colloids attached to the fracture surface. Additionally, we assume the deposition of colloids onto fracture surfaces neither changes the cross-sectional area of the fracture nor promotes clogging. Although no single filtration model can describe all reactions, Eq. (2) may be used to approximate both irreversible first order kinetics and instantaneous reversible reactions.

The formulation of Eqs. (1) and (2) is quite general and, depending on boundary and initial conditions, not amenable to an exact analytical solution. In subsequent sections, analytical solutions to various simplified versions of Eqs. (1) and (2) subject to appropriate boundary and initial conditions are derived.

2.2. Transport parameters for finitely sized colloid plumes

2.2.1. Non-attaching or reversibly attaching colloids

In this work, it is assumed that a colloid travels with a velocity corresponding to the flow velocity at its centroid due to the surrounding hydraulic gradient. Because the finite size of a colloid does not allow it to sample the slowest moving portion of the velocity profile nearest the wall, the effective velocity of a finitely sized colloid is greater than the mean fluid velocity. The effective velocity of a colloid plume has been derived by James and Chrysikopoulos [27] as

$$U_{\text{eff}} = \frac{2}{3} U_{\max} \left[1 + \frac{d_{\text{p}}}{b} - \frac{1}{2} \left(\frac{d_{\text{p}}}{b} \right)^2 \right]. \tag{5}$$

In view of Eq. (5) it is evident that the effective velocity of a colloid plume increases with increasing colloid diameter because colloids may not be larger than the fracture aperture ($d_{\text{p}}/b < 1$).

Following Taylor–Aris procedures, it is assumed that the only contributors to colloid dispersion in a fracture are the fully developed Poiseuille flow in the axial direction, transverse diffusion, and colloid–wall surface reactions. Although the parabolic velocity profile creates fluid shear in the z–direction, solutions for average colloid number concentrations derived here are independent of z because the average colloid concentration is determined by integrating the colloid concentration across the aperture of the fracture. Consequently, colloid plume movement resembles plug flow even in the presence of fully developed Poiseuille flow. The difference between a parabolic velocity profile and plug flow conditions on colloid transport lies in the spreading of the colloids. Under plug flow conditions, the molecular diffusion coefficient may be orders of magnitude smaller than the effective dispersion coefficient.

The Taylor dispersion coefficient of a non-reactive solute in a uniform fracture is given by [36,37,28]

$$\mathcal{D}_{\text{Taylor}} = \mathcal{D}_{d_{\text{p}}} + \frac{2}{945} \frac{U_{\max}^2 b^2}{\mathcal{D}_{d_{\text{p}}}}, \tag{6}$$

For finitely sized particles, a modified form of the Taylor dispersion coefficient must be used. The effective dispersion coefficient for a plume of colloids with diameter d_{p} is [27]

$$\mathcal{D}_{\text{eff}} = \mathcal{D}_{d_{\text{p}}} + \frac{2}{945} \frac{U_{\max}^2 b^2}{\mathcal{D}_{d_{\text{p}}}} \left(1 - \frac{d_{\text{p}}}{b} \right)^6. \tag{7}$$

It should be noted that Eqs. (5) and (7) are steady state values reached after a period of time on the order of colloid molecular diffusion time across the channel, which is about 10,000 s (3 h) for fractures examined in this work [38] (eq. 13).

2.2.2. Irreversibly attaching colloids

Effective parameters for solute transport in cylindrical tubes and channels with simple wall geometries subject to irreversible attachment have been derived in numerous works [16,39–41]. In this section, we present effective parameters appropriate for the transport of finitely sized colloids undergoing irreversible attachment onto fracture walls.

The first order effective decay coefficient arising from irreversible solute attachment at the fracture walls was derived by Dijk and Berkowitz [41] (within eq. 12) and it is rewritten here in dimensional form:

$$K_{\text{eff}} = \frac{12 \mathcal{D}_{d_{\text{p}}}}{b^2} \frac{Da}{6 + Da}, \tag{8}$$

where Da is the dimensionless Damköhler number measuring the ratio of the tendency for reaction over the tendency for diffusive transport, defined as [42] (p. 377)

$$Da = \frac{k_{\text{f}} b}{\mathcal{D}_{d_{\text{p}}}}, \tag{9}$$

where k_{f} is the forward filtration rate constant. Note that K_{eff} is dependent upon Da and when the attachment rate is large, colloid concentrations in the fracture approach zero and the mass transport process in the system becomes diffusion controlled [40].

The mean velocity of an irreversibly attaching solute in a fracture derived by Berkowitz and Zhou [40] (below eq. 21) is modified here to account for finitely sized colloids by substituting Eq. (5) into the dimensional form of their expression. The resulting effective velocity for a plume of finitely sized colloids undergoing irreversible attachment at the fracture walls is given as

$$U_{\text{eff}} = \frac{2}{3} U_{\max} \left[1 + \frac{d_{\text{p}}}{b} - \frac{1}{2} \left(\frac{d_{\text{p}}}{b} \right)^2 + \frac{3}{10} \frac{Da}{6 + Da} \right]. \tag{10}$$

Colloid reactions with fracture walls lead to a depletion of colloids in the slower moving portion of the velocity profile resulting in a distribution of suspended colloids weighted in favor of the colloids remaining in the faster moving region of the flow profile. Thus, suspended colloids are advected at a velocity greater than the effective velocity observed in the absence of colloid attachment.

The dispersion coefficient for an irreversibly attaching solute traveling within a water saturated fracture with uniform aperture was derived by Dijk and Berkowitz [41] (within eq. 12). Substitution of Eq. (7) into the dimensionalized form of their expression leads to the following effective dispersion coefficient for a plume of finitely sized colloids undergoing irreversible attachment at the fracture walls:

$$D_{\mathrm{eff}} = \mathcal{D}_{d_\mathrm{p}} + \frac{2}{945}\frac{U_{\max}^2}{\mathcal{D}_{d_\mathrm{p}}}\left[\left(1-\frac{d_\mathrm{p}}{b}\right)^6 - \frac{7}{10}\frac{Da}{6+Da}\right]. \tag{11}$$

From the preceding relationship, it is evident that increasing Da serves to decrease colloid spreading in a fracture. Note that if $Da=0$ (no wall reaction or $k_\mathrm{f}=0$), then Eqs. (10) and (11) reduce to Eqs. (5) and (7), respectively.

3. Analytical solutions

3.1. Instantaneous injection

3.1.1. No colloid attachment

3.1.1.1. Monodisperse colloid plume. Consider the case where a known number of monodisperse colloids are released instantaneously within a uniform, water saturated, fracture. Assuming that there are no colloid–wall interactions, Eq. (2) is eliminated from the model formulation and $n^*_{d_\mathrm{p}}=0$. A solution may be found for average colloid concentration across the fracture given by:

$$\bar{n}_{d_\mathrm{p}}(x,\ t) = \frac{1}{b}\int_{-b/2}^{b/2} n_{d_\mathrm{p}}(x,\ z,\ t)\mathrm{d}z. \tag{12}$$

Eq. (1) may be simplified through a transformation of coordinates. A quasi-steady state assumption is made by considering only advection across the plane moving with the center of mass of the colloid distribution collapsing x and t into a single coordinate thereby eliminating the transient term in Eq. (1). Let $\xi = x - U_{\mathrm{eff}}t$ represent the distance along the fracture from a fluid parcel traveling with velocity equal to the effective velocity of the colloid plume, U_{eff}, at time, t. Applying this transformation yields, after some manipulation, the familiar unsteady dispersion equation [27]:

$$\frac{\partial \bar{n}_{d_\mathrm{p}}(\xi,\ t)}{\partial t} = D_{\mathrm{eff}}\frac{\partial^2 \bar{n}_{d_\mathrm{p}}(\xi,\ t)}{\partial \xi^2}, \tag{13}$$

where D_{eff} defined in Eq. (7) describes the spreading of the plume with respect to the moving coordinate ξ. For an instantaneous injection of monodisperse colloid at the inlet of a semi-infinite fracture, the appropriate boundary and initial conditions are:

$$\bar{n}_{d_\mathrm{p}}(\pm\infty,\ t) = 0, \tag{14}$$

$$\bar{n}_{d_\mathrm{p}}(\xi,\ 0) = n_0\delta(\xi), \tag{15}$$

where n_o represents the initial number of monodisperse colloids injected into the fracture per cross-sectional area of the fracture (plane source); and $\delta(\xi)$ is the Dirac delta function. The combination of boundary and initial conditions, Eqs. (14) and (15), describe an instantaneous release of colloids. Boundary condition Eq. (14) states that the fracture system is infinite and the concentration of colloids infinitely far downstream from the inlet is always zero. Note that for the case of instantaneous colloid injection, n_o has units of colloids per cross-sectional area of the fracture while $\delta(\xi)$ has units of inverse length. The analytical solution to Eq. (13) subject to Eqs. (14) and (15) has been derived by Carslaw and Jaeger [43] (p. 259) and it is presented here as a function of the original variable $x = \xi + U_{\mathrm{eff}}t$ as follows:

$$\bar{n}_{d_\mathrm{p}}(x,\ t) = \frac{n_\mathrm{o}}{(4\pi D_{\mathrm{eff}})^{1/2}}\exp\left[\frac{(x-U_{\mathrm{eff}}t)^2}{4D_{\mathrm{eff}}t}\right]. \tag{16}$$

Although the preceding solution is well known, its physical meaning and application to the transport of finitely sized colloids through use of the new definitions of U_{eff} and D_{eff} for colloids of diameter d_p is novel.

3.1.1.2. Polydisperse colloid plume. When polydisperse colloid plumes are considered, the initial

number concentration of colloids introduced into the fracture consisting of several discrete initial number sub-concentrations of colloids with diameter d_p, $N_o(d_p)$, is used in Eq. (15). Because the boundary conditions and domain of the solution are identical for all colloids, regardless of size, the solution for each colloid size may be added.

In view of the analytical solution for a monodisperse colloid distribution given by Eq. (16) with n_o replaced by $N_o(d_p)$, the analytical solution for the polydisperse colloid distribution is obtained by summing the individual solutions corresponding to each discrete $N_o(d_p)$:

$$\bar{n}_{d_p}(x,\ t) = \sum_{d_p} \frac{N_o\left(d_p\right)}{(4\pi D_{\text{eff}})^{1/2}} \exp\left[-\frac{(x - U_{\text{eff}}t)^2}{4D_{\text{eff}}t}\right]. \tag{17}$$

For a continuous distribution of colloid diameters, the initial number concentration of polydisperse colloids is expressed as

$$n_{o_{d_p}} = \int_0^\infty n_{\text{pdf}}\,\mathrm{d}d_p, \tag{18}$$

where n_{pdf} is an appropriate probability density function for polydisperse colloids. Consequently, the analytical solution for a continuous distribution of instantaneously injected polydisperse colloids is obtained from Eq. (17) by replacing the summation with integration over the entire range of colloid sizes in the polydisperse colloid distribution and replacing $N_o(d_p)$ with $n_{o_{d_p}}$ as follows:

$$\bar{n}_{d_p}(x,\ t) = \int_0^\infty \frac{n_{\text{pdf}}}{(4\pi D_{\text{eff}})^{1/2}} \exp\left[-\frac{(x - U_{\text{eff}}t)^2}{4D_{\text{eff}}t}\right]\mathrm{d}d_p. \tag{19}$$

Employing Eqs. (5) and (7) in Eq. (19) yields an integral equation expressing the temporally and spatially varying colloid concentration of a polydisperse colloid plume within a water saturated fracture with uniform aperture that is a function of the distribution of colloid diameters. In practice, the upper limit of integration in Eq. (19) need only be evaluated to b. It should be noted that because Eq. (13) can be reformulated as an initial value problem, concentration in the fracture for any distribution of colloids introduced anywhere along the x-axis may be solved [44,45].

3.1.2. Irreversible colloid attachment

3.1.2.1. Monodisperse colloid plume. Colloids present in environmental systems have physicochemical properties that allow them to react with the media in which they reside. Consequently, colloid wall reactions (attachment) can be important processes affecting their transport. The colloid concentration attached onto fracture walls is determined through solution to Eq. (2).

The local linear irreversible rate of colloid filtration as a function of the average colloid concentration across the fracture can be expressed as [26]

$$\frac{\partial n^*_{d_p}(x,\ t)}{\partial t} = k_f \bar{n}_{d_p}(x,\ t), \tag{20}$$

where k_f is the forward filtration rate constant that is often expressed as a function of colloid diameter [46]. In view of Eq. (20), the governing Eq. (2), can be rewritten as

$$\mathcal{D}_{d_p} \frac{\partial n_{d_p}(x,\ \pm b/2,\ t)}{\partial z} = \mp k_f \bar{n}_{d_p}(x,\ t). \tag{21}$$

The preceding equation expresses the attachment of colloids onto the fracture walls as a function of average colloid concentration across the fracture, colloid diffusion coefficient, and filtration rate.

Following the work of Johns and DeGance [39], each term of the governing transport equation, Eq. (1), is averaged across the fracture according to Eq. (12), yielding the following differential equation for the average colloid concentration:

$$\frac{\partial \bar{n}_{d_p}(x,\ t)}{\partial t} = \mathcal{D}_{d_p}\left[\frac{\partial^2 \bar{n}_{d_p}(x,\ t)}{\partial x^2} + \frac{\partial n_{d_p}(x,\ \pm b/2,\ t)}{\partial z}\right] - \frac{\partial}{\partial x}\int_{-b/2}^{b/2} u(z) n_{d_p}(x,\ z,\ t)\mathrm{d}z. \tag{22}$$

Substitution of Eqs. (2) and (3) into Eq. (22) yields the following 1D advection–diffusion equation with first-order decay term [47] (Eq. (3.4))

$$\frac{\partial \bar{n}_{d_p}(x,\ t)}{\partial t} = D_{\text{eff}} \frac{\partial^2 \bar{n}_{d_p}(x,\ t)}{\partial x^2} - U_{\text{eff}} \frac{\partial \bar{n}_{d_p}(x,\ t)}{\partial x} + K_{\text{eff}} \bar{n}_{d_p}(x,\ t), \tag{23}$$

where the effective decay, advection, and dispersion constants are given by Eq. (8), Eq. (10), and Eq. (11), respectively.

Similarly to the case of no colloid attachment and following the work of James and Chrysikopoulos [27], the preceding transport equation, (Eq. 23), can be manipulated to yield the unsteady diffusion equation with decay:

$$\frac{\partial \bar{n}_{d_p}(\xi,\ t)}{\partial t} = D_{\text{eff}} \frac{\partial^2 \bar{n}_{d_p}(\xi,\ t)}{\partial \xi^2} - K_{\text{eff}} \bar{n}_{d_p}(\xi,\ t). \tag{24}$$

Substituting $\bar{n}_{d_p}(\xi,\ t) = \hat{\bar{n}}_{d_p} \exp(-K_{\text{eff}} t)$ into the preceding equation results in an equation equivalent to Eq. (13) in $\hat{\bar{n}}_{d_p}$ where the effective decay and dispersion constants are given by Eqs. (8) and (11), respectively.

Upon back substitution of the transformed average colloid concentration, the solution to Eq. (24) subject to boundary and initial conditions Eqs. (14) and (15) is

$$\bar{n}_{d_p}(x,\ t) = \frac{n_o}{(4\pi D_{\text{eff}} t)^{1/2}} \exp\left[-K_{\text{eff}} t - \frac{(x - U_{\text{eff}} t)^2}{4 D_{\text{eff}} t}\right]. \tag{25}$$

3.1.2.2. Polydisperse colloid plume. In view of Eq. (18), the analytical solution, Eq. (25), for monodisperse colloids, replacing n_o with $n_{o_{d_p}}$, is integrated to yield

$$\bar{n}d_p(x,\ t) = \int_0^\infty \frac{n_{\text{pdf}}}{(4\pi D_{\text{eff}} t)^{1/2}} \times \exp\left[-K_{\text{eff}} t - \frac{(x - U_{\text{eff}} t)^2}{4 D_{\text{eff}} t}\right] \mathrm{d}d_p, \tag{26}$$

where K_{eff}, U_{eff}, and D_{eff} are defined in Eq. (8), Eq. (10), and Eq. (11), respectively.

3.1.3. Reversible colloid attachment

3.1.3.1. Monodisperse colloid plume. Changes in interstitial solution chemistry or varied hydraulic gradients within the fracture may contribute to the resuspension of previously deposited colloids. Consequently, we consider the case where colloids are allowed to reversibly attach onto fracture walls. It is assumed that local chemical equilibrium exists throughout the system. For simplicity, the following linear isotherm is used to express the relationship between the average number of colloids in solution and the number of colloids attached onto the solid surface

$$n^*_{d_p}(x,\ t) = k_r \bar{n}_{d_p}(x,\ t), \tag{27}$$

where k_r is the surface distribution coefficient. Taking the derivative of both sides of Eq. (27) with respect to time yields the desired expression for the time dependent attachment of colloids onto the fracture surface

$$\frac{\partial n^*_{d_p}(x,\ t)}{\partial t} = k_r \frac{\partial \bar{n}_{d_p}(x,\ t)}{\partial t}. \tag{28}$$

There is no closed form analytical solution to the coupled governing Eqs. (1) and (2), subject to a constant concentration of colloids at the inlet and reversible wall attachment. However, for the special case where the colloid concentration is averaged across the fracture (eliminating the z coordinate), the following 1D advection–dispersion equation approximates the transport of finitely sized colloids along a uniform aperture fracture [48] (p. 477):

$$\frac{\partial \bar{n}_{d_p}(x,\ t)}{\partial t} + \frac{2}{b}\frac{\partial n^*_{d_p}(x,\ t)}{\partial t} = D_{\text{eff}} \frac{\partial^2 \bar{n}_{d_p}(x,\ t)}{\partial x^2} - U_{\text{eff}} \frac{\partial \bar{n}_{d_p}(x,\ t)}{\partial x}. \tag{29}$$

The preceding equation is a consequence of mass conservation applied to the average colloid concentration within the fracture. It is a better approximation at larger distances and times because the relative effects of axial molecular diffusion on the solution become negligible. The factor of two in front of the rate of change of attached colloids per unit fracture surface area arises from colloids reversibly attaching onto both walls of the fracture. Substituting Eq. (28) into Eq. (29) yields

$$R\frac{\partial \bar{n}_{d_p}(x,\ t)}{\partial t} = D_{\text{eff}} \frac{\partial^2 \bar{n}_{d_p}(x,\ t)}{\partial x^2} - U_{\text{eff}} \frac{\partial \bar{n}_{d_p}(x,\ t)}{\partial x}, \tag{30}$$

where U_{eff} and D_{eff} are given by Eqs. (5) and (7), respectively; and the retardation factor, R, is given by

$$R = 1 + 2\frac{k_r}{b}. \tag{31}$$

Using the same coordinate transfer used to generate Eq. (13), Eq. (30) is reformulated as

$$R\frac{\partial \bar{n}_{d_p}(\xi,\ t)}{\partial t} = D_{\text{eff}} \frac{\partial^2 \bar{n}_{d_p}(\xi,\ t)}{\partial \xi^2}, \tag{32}$$

which, subject to Eqs. (14) and (15), has solution

$$\bar{n}_{d_p}(x,\ t) = \frac{n_o}{(4\pi D_{eff} t)^{1/2}} \exp\left[-\frac{(Rx - U_{eff}t)^2}{4RD_{eff}t}\right], \tag{33}$$

that accounts for finitely sized colloids through U_{eff} and D_{eff}. Note that when there is no wall reaction ($k_r = 0$), the retardation factor is one and Eq. (33) reduces to Eq. (16).

3.1.3.2. Polydisperse colloid plume. In view of Eq. (18) and replacing n_o with $n_{o_{d_p}}$, the analytical solution, Eq. (33), for monodisperse colloids using the size dependent effective velocity and effective dispersion coefficient given by Eqs. (5) and (7), respectively, is integrated yielding the following expression for the time and space dependent number concentration of polydisperse colloids subject to linear reversible attachment at the fracture walls

$$\bar{n}_{d_p}(x,\ t) = \int_0^\infty \frac{n_{pdf}}{(4\pi D_{eff} t)^{1/2}} \times \exp\left[-\frac{(Rx - U_{eff}t)^2}{4RD_{eff}t}\right] \mathrm{d}d_p. \tag{34}$$

3.2. Constant concentration injection

3.2.1. No colloid attachment

3.2.1.1. Monodisperse colloid plume. Berkowitz and Zhou [40] have presented a solution for the specific case of solute transport in a channel formed between two parallel plates with a constant concentration inlet boundary condition. In this section, their model is extended to the more general case of transport of finitely sized, monodisperse colloids given constant concentration injection. The unsteady dispersion equation, Eq. (13), is again solved analytically for an average colloid concentration across the fracture (and not the local n_{d_p}). For the case when a fracture is initially free of colloids, with a constant concentration of colloids at the inlet, and without colloid reactions at the fracture walls, the appropriate boundary and initial conditions are:

$$\bar{n}_{d_p}(0,\ t) = n_o, \tag{35}$$

$$\bar{n}_{d_p}(\infty,\ t) = 0, \tag{36}$$

$$\bar{n}_{d_p}(\xi,\ 0) = 0, \tag{37}$$

where n_o is the total number of monodisperse colloids per unit fracture volume (concentration). The analytical solution to Eq. (13) subject to Eqs. (35)–(37) may be found using Laplace transform techniques [49]. It is presented here in a form that accounts for the finite size of the colloids as

$$\bar{n}(x,\ t) = \frac{n_o}{2}\left\{\mathrm{erfc}\left[\frac{x - U_{eff}t}{2(D_{eff}t)^{1/2}}\right] + \exp\left(\frac{xU_{eff}}{D_{eff}}\right) \times \mathrm{erfc}\left[\frac{x + U_{eff}t}{2(D_{eff}t)^{1/2}}\right]\right\}, \tag{38}$$

where U_{eff} and D_{eff} are given by Eqs. (5) and (7), respectively.

3.2.1.2. Polydisperse colloid plume. Replacing n_o with $n_{o_{d_p}}$ and using Eq. (18), the analytical solution, Eq. (38), for monodisperse colloids is integrated to yields the normalized concentration of polydisperse colloids in the absence of colloid attachment onto the fracture walls:

$$\bar{n}_{d_p}(x,\ t) = \frac{1}{2}\int_0^\infty n_{pdf}\left\{\mathrm{erfc}\left[\frac{x - U_{eff}t}{2(D_{eff}t)^{1/2}}\right] + \exp\left(\frac{xU_{eff}}{D_{eff}}\right)\mathrm{erfc}\left[\frac{x + U_{eff}t}{2(D_{eff}t)^{1/2}}\right]\right\} \mathrm{d}d_p. \tag{39}$$

The size dependent values for the effective velocity and effective dispersion coefficient given by Eqs. (5) and (7), respectively, should be used in the preceding equation. In both Eqs. (38) and (39), the term involving the exponential function is non-zero only for small x or t where axial molecular diffusion affects the solution.

3.2.2. Irreversible colloid attachment

3.2.2.1. Monodisperse colloid plume. Performing the same integration across the fracture aperture as in Eq. (22) with subsequent substitution of Eqs. (3) and (2) yields the following 1D advection–diffusion equation with first order decay term

$$\frac{\partial \bar{n}_{d_p}(x,\ t)}{\partial t} = D_{eff}\frac{\partial^2 \bar{n}_{d_p}(x,\ t)}{\partial x^2} - U_{eff}\frac{\partial \bar{n}_{d_p}(x,\ t)}{\partial x} - K_{eff}\bar{n}_{d_p}(x,\ t), \tag{40}$$

where the effective decay, advection, and dispersion constants are given by Eq. (8), Eq. (10), and Eq. (11), respectively.

The solution to Eq. (40) subject to the following constant concentration inlet boundary and initial conditions

$$\bar{n}_{d_p}(0,\ t) = n_o, \tag{41}$$

$$\bar{n}_{d_p}(\infty,\ t) = 0, \tag{42}$$

$$\bar{n}_{d_p}(x,\ 0) = 0, \tag{43}$$

is given by Berkowitz and Zhou [40], (Eq. (21)):

$$\bar{n}(x,t) = \frac{n_o}{2}\exp\left(\frac{xU_{\text{eff}}}{2D_{\text{eff}}}\right)\left\{\exp\left(-\frac{\Omega x}{2D_{\text{eff}}}\right)\times \operatorname{erfc}\left[\frac{x-\Omega t}{2(D_{\text{eff}}t)^{1/2}}\right] + \exp\left(\frac{\Omega x}{2D_{\text{eff}}}\right)\times \operatorname{erfc}\left[\frac{x+\Omega t}{2(D_{\text{eff}}t)^{1/2}}\right]\right\}, \tag{44}$$

$$\Omega = \left(U_{\text{eff}}^2 + 4K_{\text{eff}}D_{\text{eff}}\right)^{1/2}, \tag{45}$$

where, for the case of finitely sized colloids undergoing irreversible attachment at the fracture walls considered here, K_{eff}, U_{eff}, and D_{eff} are given by Eq. (8), Eq. (10), and Eq. (11), respectively.

3.2.2.2. Polydisperse colloid plume. In view of Eq. (18), the analytical solution, Eq. (44), for monodisperse colloids, replacing n_o, with $n_{o_{d_p}}$, is integrated to yield

$$\bar{n}_{d_p}(x,t) = \frac{1}{2}\int_0^\infty n_{\text{pdf}}\exp\left(\frac{xU_{\text{eff}}}{2D_{\text{eff}}}\right)\times\left\{\exp\left(-\frac{\Omega x}{2D_{\text{eff}}}\right)\operatorname{erfc}\left[\frac{x-\Omega t}{2(D_{\text{eff}}t)^{1/2}}\right] + \exp\left(\frac{\Omega x}{2D_{\text{eff}}}\right)\operatorname{erfc}\left[\frac{x+\Omega t}{2(D_{\text{eff}}t)^{1/2}}\right]\right\}\mathrm{d}d_p \tag{46}$$

where K_{eff}, U_{eff}, D_{eff}, and Ω are defined in Eq. (8), Eq. (10), Eq. (11), and Eq. (45), respectively. The second term inside the integral of the preceding equation rapidly diminishes for increasing x or t.

3.2.3. Reversible colloid attachment

3.2.3.1. Monodisperse colloid plume. The solution to Eq. (30) subject to boundary and initial conditions Eqs. (41)–(43) was tabulated by van Genuchten and Alves [49] and it is presented here in a form that accounts for finitely sized colloids

$$\bar{n}_{d_p}(x,\ t) = \frac{n_o}{2}\left\{\operatorname{erfc}\left[\frac{Rx-U_{\text{eff}}t}{2(RD_{\text{eff}}t)^{1/2}}\right] + \exp\left(\frac{xU_{\text{eff}}}{D_{\text{eff}}}\right)\operatorname{erfc}\left[\frac{Rx+U_{\text{eff}}t}{2(RD_{\text{eff}}t)^{1/2}}\right]\right\}, \tag{47}$$

through U_{eff} and D_{eff} which are given by Eqs. (5) and (7), respectively. Note that when there is no wall reaction ($k_r = 0$) the retardation factor is one and Eq. (47) reduces to Eq. (38).

3.2.3.2. Polydisperse colloid plume. Replacing n_o by $n_{o_{d_p}}$ defined by Eq. (18), using the size dependent effective velocity effective dispersion given by Eqs. (5) and (7), respectively, and integrating Eq. (47) over all colloid sizes results in the following expression for number concentration of polydisperse colloids subject to linear reversible attachment at the fracture walls

$$\bar{n}_{d_p}(x,\ t) = \frac{1}{2}\int_0^\infty n_{\text{pdf}}\left\{\operatorname{erfc}\left[\frac{Rx-U_{\text{eff}}t}{2(RD_{\text{eff}}t)^{1/2}}\right] + \exp\left(\frac{xU_{\text{eff}}}{D_{\text{eff}}}\right)\operatorname{erfc}\left[\frac{Rx+U_{\text{eff}}t}{2(RD_{\text{eff}}t)^{1/2}}\right]\right\}\mathrm{d}d_p. \tag{48}$$

A summary of all governing equations, boundary, and initial conditions employed for each case, and their respective solutions is presented for polydisperse colloids subject to instantaneous injection in Table 1 and a constant concentration inlet boundary condition in Table 2. Note that any appropriate probability density function n_{pdf} can be employed with the analytical solutions for polydisperse colloid transport in saturated fractures derived here.

4. Discussion

Colloids found in natural environments are generally not of a single size; rather, they have a distribution of sizes [50,51]. Ledin et al. [52] measured naturally occurring colloids in deep groundwater from Äspö, Sweden and determined them to have a log-normal

Table 1
Analytical solutions for polydisperse colloid transport in saturated fractures subject to an instantaneous inlet boundary condition

Model	Analytical solution
$\frac{\partial \bar{n}_{d_p}(\xi,t)}{\partial t} = D_{\text{eff}} \frac{\partial^2 \bar{n}_{d_p}(\xi,t)}{\partial \xi^2}$	$\bar{n}_{d_p}(x,t) = \int_0^\infty \frac{n_{\text{pdf}}}{(4\pi D_{\text{eff}} t)^{1/2}} \exp\left[-\frac{(x-U_{\text{eff}}t)^2}{4D_{\text{eff}}t}\right] \mathrm{d}d_p$
$\xi = x - U_{\text{eff}} t$	$U_{\text{eff}} = \frac{2}{3}U_{\max}\left[1 + \frac{d_p}{b} - \frac{1}{2}\left(\frac{d_p}{b}\right)^2\right]$
	$D_{\text{eff}} = \mathcal{D}_{d_p} + \frac{2}{945}\frac{U_{\max}^2 b^2}{\mathcal{D}_{d_p}}\left(1-\frac{d_p}{b}\right)^6$
$\frac{\partial \bar{n}_{d_p}(\xi,t)}{\partial t} = D_{\text{eff}} \frac{\partial^2 \bar{n}_{d_p}(\xi,t)}{\partial \xi^2} - K_{\text{eff}} \bar{n}_{d_p}(\xi,t)$	$\bar{n}_{d_p}(x,t) = \int_0^\infty \frac{n_{\text{pdf}}}{(4\pi D_{\text{eff}} t)^{1/2}} \exp\left[-K_{\text{eff}}t - \frac{(x-U_{\text{eff}}t)^2}{4D_{\text{eff}}t}\right] \mathrm{d}d_p$
$\xi = x - U_{\text{eff}} t$	$U_{\text{eff}} = \frac{2}{3}U_{\max}\left[1 + \frac{d_p}{b} - \frac{1}{2}\left(\frac{d_p}{b}\right)^2 + \frac{3}{10}\frac{Da}{6+Da}\right]$
	$D_{\text{eff}} = \mathcal{D}_{d_p} + \frac{2}{945}\frac{U_{\max}^2 b^2}{\mathcal{D}_{d_p}}\left[\left(1-\frac{d_p}{b}\right)^6 - \frac{7}{10}\frac{Da}{6+Da}\right]$
	$K_{\text{eff}} = \frac{12\mathcal{D}_{d_p}}{b^2}\frac{Da}{6+Da}$
$\frac{\partial \bar{n}_{d_p}(\xi,t)}{\partial t} = D_{\text{eff}} \frac{\partial^2 \bar{n}_{d_p}(\xi,t)}{\partial \xi^2}$	$\bar{n}_{d_p}(x,t) = \int_0^\infty \frac{n_{\text{pdf}}}{(4\pi D_{\text{eff}} t)^{1/2}} \exp\left[-\frac{(Rx-U_{\text{eff}}t)^2}{4RD_{\text{eff}}t}\right] \mathrm{d}d_p$
$\xi = x - \frac{U_{\text{eff}} t}{R}$	$U_{\text{eff}} = \frac{2}{3}U_{\max}\left[1 + \frac{d_p}{b} - \frac{1}{2}\left(\frac{d_p}{b}\right)^2\right]$
	$D_{\text{eff}} = \mathcal{D}_{d_p} + \frac{2}{945}\frac{U_{\max}^2 b^2}{\mathcal{D}_{d_p}}\left(1-\frac{d_p}{b}\right)^6$
	$R = 1 + 2\frac{k_r}{b}$

distribution of diameters given by:

$$n_{\text{pdf}} = \frac{n_o}{\sqrt{2\pi}\zeta d_p} \exp\left[-\frac{1}{2}\left(\frac{\ln d_p - \lambda}{\zeta}\right)^2\right], \qquad (49)$$

where λ is the mean of colloid log-diameters; ζ^2 is the variance of the colloid log-diameters. In this work the mean colloid diameter is represented by $\mu = \exp(\lambda + 0.5\zeta^2)$ and the standard deviation of the colloid diameter by $\sigma = \mu(e^{\zeta^2}-1)^{1/2}$ [53]. The initial concentration of polydisperse colloid in a plume is determined by integrating the preceding equation over all colloid diameters in the distribution.

For the model simulation presented in this work four different colloid distributions consisting of $n_o = n_{o_{d_p}} = 10{,}000$ colloids m^{-3} are considered—well below the limit of 10^{16} colloids m^{-3} where colloid–colloid interactions affect their transport [54]. One distribution is composed of monodisperse colloids with diameter $d_p = 1$ μm. The other three polydisperse colloid distributions comprise colloids with log-normally distributed diameters, all with mean colloid diameter $\mu = 1$ μm, but increasing standard deviations of $\sigma = 0.3$, 0.6 and 0.9 μm. It is assumed that the fracture has an aperture of $b = 1 \times 10^{-4}$ m and the maximum centerline velocity of tile interstitial fluid is $U_{\max} = 1 \times 10^{-6}$ m s^{-1}, corresponding to values typical of fractured subsurface media [55]. The results from the model simulations are presented as space and time dependent colloid concentrations in the form of snapshots in time, or breakthrough curves. The snapshots are taken after 5,000 h of transport time in the system, while the breakthrough curves are provided at a distance of 12 m from the colloid injection point. Note that for a Poiseuille velocity profile with $U_{\max} = 1 \times 10^{-6}$, m s^{-1}, parcel of fluid moving with the average velocity will travel 12 m in 5,000 h.

Table 2
Analytical solutions for polydisperse colloid transport in saturated fractures subject to a constant concentration inlet boundary condition

Model	Analytical solution
$\frac{\partial \bar{n}_{d_p}(\xi,t)}{\partial t} = D_{\text{eff}} \frac{\partial^2 \bar{n}_{d_p}(\xi,t)}{\partial \xi^2}$	$\bar{n}_{d_p}(x,t) = \frac{1}{2}\int_0^\infty n_{\text{pdf}} \left\{ \text{erfc}\left[\frac{x - U_{\text{eff}} t}{2(D_{\text{eff}} t)^{1/2}}\right] + \exp\left(\frac{xU_{\text{eff}}}{D_{\text{eff}}}\right) \text{erfc}\left[\frac{x + U_{\text{eff}} t}{2(D_{\text{eff}} t)^{1/2}}\right] \right\} \mathrm{d}d_{\text{p}}$
$\xi = x - U_{\text{eff}} t$	$U_{\text{eff}} = \frac{2}{3} U_{\max} \left[1 + \frac{d_{\text{p}}}{b} - \frac{1}{2}\left(\frac{d_{\text{p}}}{b}\right)^2\right]$
	$D_{\text{eff}} = \mathcal{D}_{d_{\text{p}}} + \frac{2}{945} \frac{U_{\max}^2 b^2}{\mathcal{D}_{d_{\text{p}}}} \left(1 - \frac{d_{\text{p}}}{b}\right)^6$
$\frac{\partial \bar{n}_{d_p}(x,t)}{\partial t} = D_{\text{eff}} \frac{\partial^2 \bar{n}_{d_p}(x,t)}{\partial x^2} - U_{\text{eff}} \frac{\partial \bar{n}_{d_p}(x,t)}{\partial x} - K_{\text{eff}} \bar{n}_{d_p}(x,t)$	$\bar{n}_{d_p}(x,t) = \frac{1}{2}\int_0^\infty n_{\text{pdf}} \exp\left(\frac{xU_{\text{eff}}}{2D_{\text{eff}}}\right) \times \left\{ \exp\left(-\frac{\Omega x}{2D_{\text{eff}}}\right) \times \text{erfc}\left[\frac{x - \Omega t}{2(D_{\text{eff}} t)^{1/2}}\right] + \exp\left(\frac{\Omega x}{2D_{\text{eff}}}\right) \text{erfc}\left[\frac{x + \Omega t}{2(D_{\text{eff}} t)^{1/2}}\right] \right\} \mathrm{d}d_{\text{p}}$
	$\Omega = (U_{\text{eff}}^2 + 4K_{\text{eff}} D_{\text{eff}})^{1/2}$
	$U_{\text{eff}} = \frac{2}{3} U_{\max} \left[1 + \frac{d_{\text{p}}}{b} - \frac{1}{2}\left(\frac{d_{\text{p}}}{b}\right)^2 + \frac{3}{10}\frac{Da}{6 + Da}\right]$
	$D_{\text{eff}} = \mathcal{D}_{d_{\text{p}}} + \frac{2}{945} \frac{U_{\max}^2 b^2}{\mathcal{D}_{d_{\text{p}}}} \left[\left(1 - \frac{d_{\text{p}}}{b}\right)^6 - \frac{7}{10}\frac{Da}{6 + Da}\right]$
	$K_{\text{eff}} = \frac{12\mathcal{D}_{d_{\text{p}}}}{b^2} \frac{Da}{6 + Da}$
$R\frac{\partial \bar{n}_{d_p}(x,t)}{\partial t} = D_{\text{eff}} \frac{\partial^2 \bar{n}_{d_p}(x,t)}{\partial x^2} - U_{\text{eff}} \frac{\partial \bar{n}_{d_p}(x,t)}{\partial x}$	$\bar{n}_{d_p}(x,t) = \frac{1}{2}\int_0^\infty n_{\text{pdf}} \left\{ \text{erfc}\left[\frac{Rx - U_{\text{eff}} t}{2(\text{R} D_{\text{eff}} t)^{1/2}}\right] + \exp\left(\frac{xU_{\text{eff}}}{D_{\text{eff}}}\right) \text{erfc}\left[\frac{Rx + U_{\text{eff}} t}{2(RD_{\text{eff}} t)^{1/2}}\right] \right\} \mathrm{d}d_{\text{p}}$
	$U_{\text{eff}} = \frac{2}{3} U_{\max} \left[1 + \frac{d_{\text{p}}}{b} - \frac{1}{2}\left(\frac{d_{\text{p}}}{b}\right)^2\right]$
	$D_{\text{eff}} = \mathcal{D}_{d_{\text{p}}} + \frac{2}{945} \frac{U_{\max}^2 b^2}{\mathcal{D}_{d_{\text{p}}}} \left(1 - \frac{d_{\text{p}}}{b}\right)^6$
	$R = 1 + 2\frac{k_{\text{r}}}{b}$

Fig. 2(a) illustrates snapshots of n_{d_p} evaluated by Eq. (16) for the monodisperse and by Eq. (19) for the polydisperse colloid distributions 5000 h after instantaneous injection because of the instantaneous inlet boundary condition, colloid concentration is presented rather than normalized colloid concentration. Note that the shape of the concentration profile change with the value of σ. A large σ implies a wide range of colloid diameters with a many number of small colloids and a few large colloids. These few largest colloids experience the greatest mean velocity and travel at the front of the concentration curve. Conversely, the many small colloids contribute to a slower moving peak concentration that lags the peak concentration of the monodisperse distribution. Fig. 2(b) shows normalized breakthrough curves evaluated by Eqs. (16) and (19) 12 m from the instantaneous injection point. Because of the increased range of colloid sizes for plumes with larger σ, the colloid distribution with $\sigma = 0.9$ μm contains the largest and smallest, colloids considered. The early initial breakthrough of this plume is attributed to the increased effective velocity of the largest colloids while complete breakthrough of this plume is delayed because of the many small colloids.

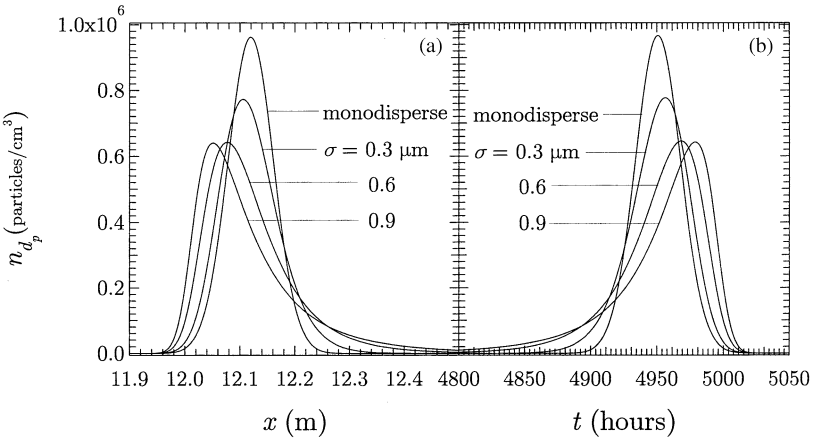

Fig. 2. Colloid concentration (a) snapshots and (b) breakthrough curves generated from Eqs. (16) and (19) for 10,000 colloids instantaneously injected at $t=0$ into a fracture with $U_{max}=1\times10^{-6}$ m s^{-1} and $b=1\times10^{-4}$ m. Three of the plumes are polydisperse and consist of colloids with log-normally distributed diameters of $\mu=1$ μm and $\sigma=0.3$, 0.6 and 0.9 μm, while the fourth plume is monodisperse with colloids with diameter 1 μm. The snapshots of colloid concentrations were evaluated 5,000 h after injection and breakthrough curves were determined 12 m downstream from the colloid injection location.

Colloid concentration snapshots evaluated by Eq. (25) for the monodisperse and by Eq. (26) for the polydisperse colloid distributions subject to instantaneous concentration injection and irreversible colloid attachment onto the fracture walls are shown in Fig. 3(a). Compared to Fig. 2, the colloid plumes in Fig. 3 show decreased concentrations (note scale change oil abscissa) and a slight increase in velocity according to Eq. (10). A constant Domköhler number of 10^{-3} was used in these simulations because larger values imply a larger K_{eff} with possible deposition of entire size ranges by 5,000 h. Selecting a constant Domköhler number results in a forward filtration rate coefficient, k_f, that is a function of colloid size. Because the Domköhler number, Eq. (9), describes the relative effect of reaction to that of molecular diffusion on colloid transport and because a smaller colloid has a larger molecular diffusion rate, a small colloid will have a proportionally large forward filtration rate coefficient (inversely proportional to the colloid

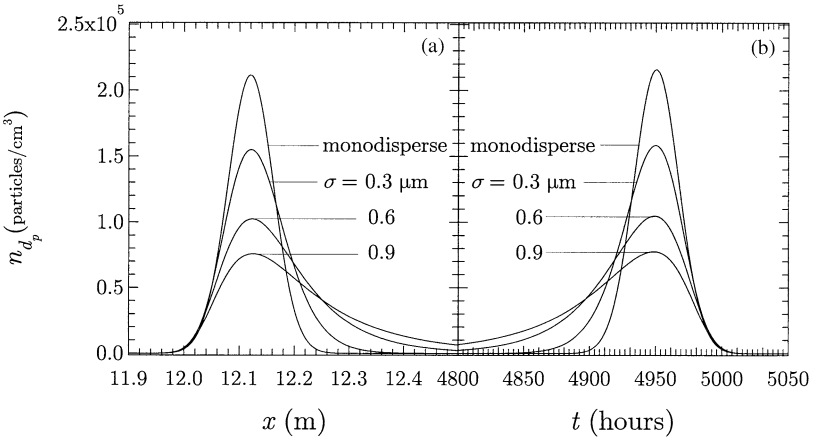

Fig. 3. Colloid concentration (a) snapshots and (b) breakthrough curves generated from Eqs. (25) and (26) for instantaneous injection and irreversible filtration (here $U_{max}\times10^{-6}$ m s^{-1}, $b=1\times10^{-4}$ m, $Da=1\times10^{-3}$, and $t=5000$ h or $x=12$ m).

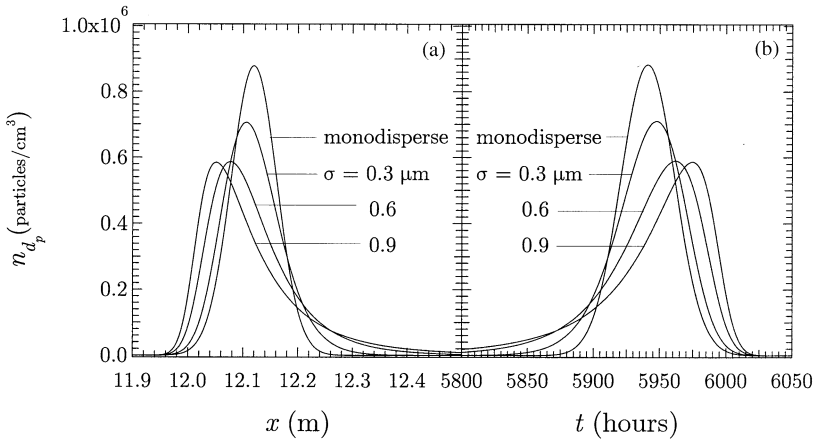

Fig. 4. Colloid concentration (a) snapshots and (b) breakthrough curves evaluated by Eqs. (33) and (34) for instantaneous injection and reversible filtration (here $U_{max} = 1 \times 10^{-6}$ m s^{-1}, $b = 1 \times 10^{-4}$ m, $k_r = 1 \times 10^{-5}$, and $t = 5{,}000$ h or $x = 12$ m).

diameter). Note the decreasing colloid concentration with increasing σ (more small colloids) of the injected colloid distribution Fig. 3(b) illustrates the colloid breakthrough curves evaluated from Eqs. (25) and (26). It is evident that increasing σ leads to increased colloid attachment onto the fracture walls. The plume with the highest σ contains the greatest number of small colloids (with large k_f). Small colloids with large forward filtration rate coefficients preferentially attach onto the fracture walls leading to a decreased plume concentration for the colloid distribution with the largest σ at a distance of 12 m from injection.

The colloid concentrations evaluated by Eq. (33) for the monodisperse and by Eq. (34) for the polydisperse colloid distributions subject to instantaneous injection and reversible attachment after 5,000 h of simulation time are shown in Fig. 4(a). A retardation factor of $R = 1.2$ with $k_r = 1 \times 10^{-5}$ m was used. The reversible attachment process serves to retard the propagation of the colloid concentration fronts (note the decreased colloid concentrations between Fig. 2(a) and Fig. 4(a) at 12 m). Fig. 4(b) illustrates the four colloid concentration plumes evaluated by Eqs. (33) and (34). It should be noted that for the conditions

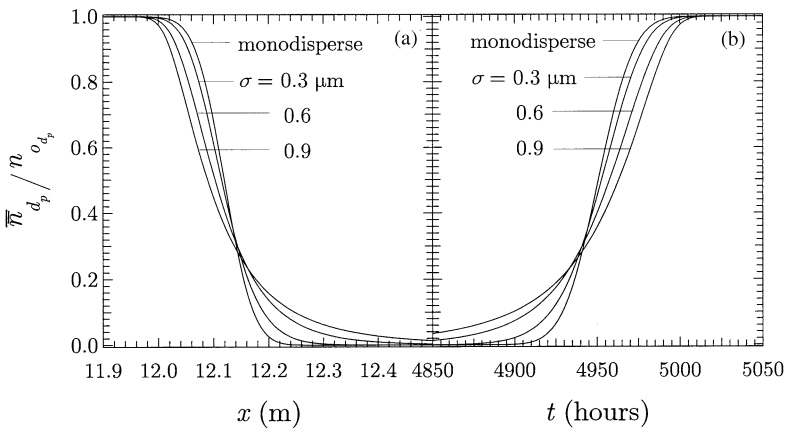

Fig. 5. Normalized colloid concentration (a) snapshots and (b) breakthrough curves evaluated by Eqs. (38) and (39) for a constant concentration inlet boundary condition accounting for reversible colloid–wall reactions (here $U_{max} = 1 \times 10^{-6}$ m s^{-1}, $b = 1 \times 10^{-4}$ m, $k_r = 1 \times 10^{-5}$, and $t = 5{,}000$ h or $x = 12$ m).

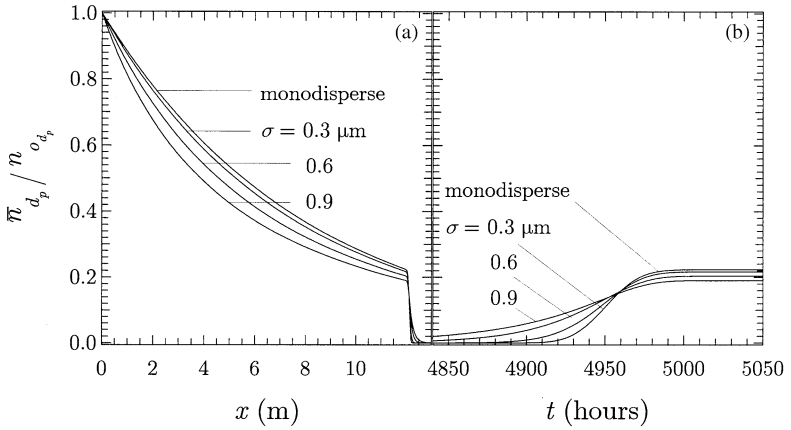

Fig. 6. Normalized colloid concentration (a) snapshots and (b) breakthrough curves evaluated by Eqs. (44) and (46) for a constant concentration inlet boundary condition accounting for irreversible colloid–wall reaction (here $U_{max} = 1 \times 10^{-6}$ m s^{-1}, $b = 1 \times 10^{-4}$ m, $Da = 1 \times 10^{-3}$, and $t = 5{,}000$ h or $x = 12$ m).

considered here, the time required for the colloid plumes to achieve complete breakthrough at a distance of 12 m from the colloid injection point is greater than for the case of non-attaching colloids shown in Fig. 2(b).

Fig. 5(a) shows normalized colloid concentration fronts evaluated by Eq. (38) for the monodisperse and by Eq. (39) for the polydisperse colloid distributions 5,000 h after the initiation of constant concentration injection. Note that the steepest concentration front is exhibited by the monodisperse colloid distribution. Increasing σ increases the dispersion of the plume because polydisperse plumes have a greater range of effective colloid velocities and effective dispersion coefficients. The corresponding normalized colloid concentration breakthrough curves 12 m from the fracture inlet are evaluated by Eq. (38) or Eq. (39) are illustrated in Fig. 5(b). Again, note the increasing dispersion of colloid distributions with increasing standard deviation.

Normalized colloid concentration fronts evaluated by Eq. (44) for the monodisperse and by Eq. (46) for

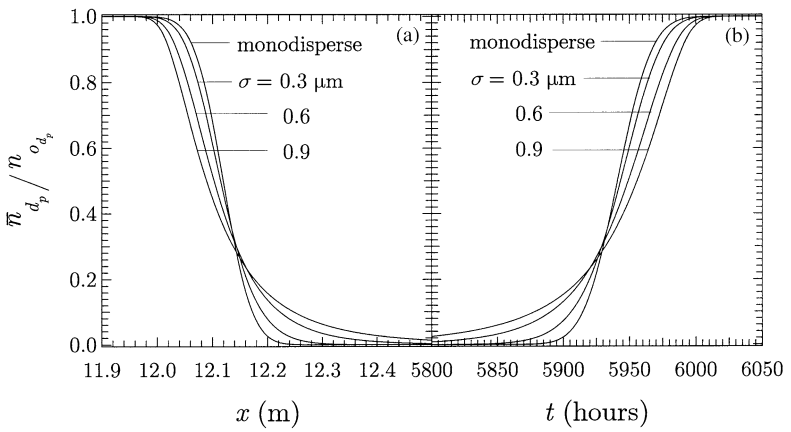

Fig. 7. Normalized colloid concentration (a) snapshots and (b) breakthrough curves evaluated by Eqs. (47) and (48) for a constant concentration inlet boundary condition accounting for reversible colloid–wall reaction (here $U_{max} = 1 \times 10^{-6}$ m s^{-1}, $b = 1 \times 10^{-4}$ m, and $k_r = 1 \times 10^{-5}$ m, and $t = 5{,}000$ h or $x = 12$ m).

the polydisperse colloid distributions subject to constant concentration injection and irreversible colloid attachment ($Da = 1 \times 10^{-3}$) are shown in Fig. 6(a). Similarly to the case with instantaneous injection and irreversible attachment, there is decreasing colloid concentration with increasing σ, Fig. 6(b) illustrates the colloid breakthrough curves evaluated from Eqs. (44) and (46). Again, increasing σ results in increased colloid attachment.

The normalized colloid concentration fronts evaluated by Eq. (47) for the monodisperse and by Eq. (48) for the polydisperse colloid distributions subject to constant concentration injection and reversible attachment after 5,000 h are shown in Fig. 7(a). Again, a retardation factor of $R = 1.2$ with $k_r = 1 \times 10^{-5}$ m was employed. The reversible attachment process serves retards the propagation of the colloid concentration fronts. Fig. 7(b) illustrates four normalized colloid concentration breakthrough curves evaluated by Eqs. (47) and (48). Note the increased time required for the colloids to reach 12 m compared to Fig. 5(b).

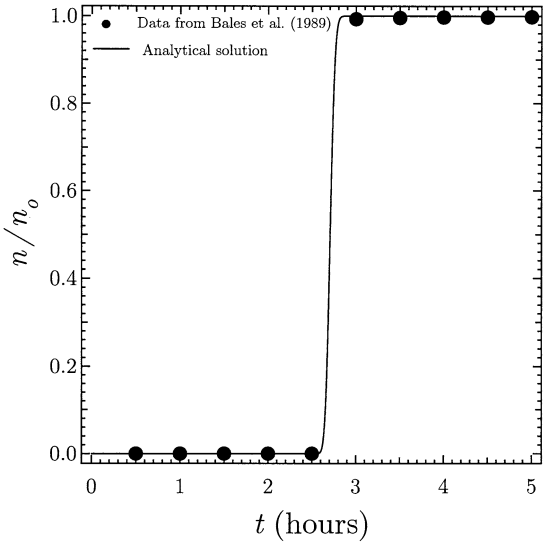

Fig. 8. Comparison of experimental data from Bales et al. [56] and the analytical solution Eq. (38) for *f*2 coliphage (monodisperse colloids plume) transport in a natural fracture in the absence of colloid–wall reaction (here $b = 1.33 \times 10^{-4}$ m, $d_p = 2.3 \times 10^{-8}$ m, $\bar{U} = 2U_{max}/3 = 1.83 \times 10^{-5}$ m s^{-1}, and $x = 0.19$ m).

5. Comparison with experimental data

An effort has been made to compare the analytical results derived in this work to available experimental data. Unfortunately, no experimental data could be found for the case of polydisperse colloid transport. However, Bales et al. [56] have experimentally studied virus transport in fractured rock. In their experiment a constant concentration of suspended *f*2 coliphages (diameter 2.3×10^{-8} m) was introduced at the inlet of a 19 cm long natural fracture at a volumetric flow rate of 1.83×10^{-10} m^3 s^{-1}. The effective cross-sectional area of the fracture was calculated by dividing the estimated volume of the fracture by the measured effective aperture and found to be 8.65×10^{-6} m^2. Although the effective porosity was reported as 0.23, the coliphages are considered large enough that penetration of the rock matrix is negligible. This experimental procedure can be most accurately compared to the solution for a constant concentration injection of monodisperse colloids without reaction at the fracture walls given by Eq. (38) with U_{eff} and D_{eff} evaluated by Eqs. (5) and (7), respectively. Because the experimental fracture was of natural rock with non-uniform aperture, the analytical results based on a uniform fracture may not be directly applicable to this case. Nevertheless, a least squares procedure [57] was used to fit the experimental data using the calculated effective cross-sectional area of the fracture as the dependent variable. This procedure yielded an estimate of 1.00×10^{-5} m^2 for the effective cross-sectional fracture area, similar to the one suggested by Bales et al. [56]. Dividing the volumetric flow rate by the fitted value of the effective cross-sectional area yields a mean fluid velocity within the fracture of $\bar{U} = 2U_{max}/3 = 1.83 \times 10^{-5}$ m s^{-1}. Fig. 8 clearly shows a good agreement between the model prediction (solid curve) and the experimental data (bullets). It is expected that if the coliphages were considered infinitesimally small that their effective velocity would decrease and their dispersivity increase according to Eqs. (5) and (7), respectively, resulting in a decreased estimate of cross-sectional area required to match the experimental data.

6. Summary

Analytical solutions describing the transport of monodisperse and polydisperse colloid plumes through a single fracture with uniform aperture accounting for

an axial parabolic velocity profile, molecular diffusion, and colloid-wall reaction are derived. It is shown that the finite size of colloids influences the effective velocity of a colloid plume. Also, because the molecular diffusion coefficient of a colloid is inversely proportional to the colloid diameter according to the Stokes–Einstein equation, and because dispersion is dependent on the velocity profile, aperture, and molecular diffusion rate, colloid size also affects the overall rate of dispersion of the colloid plume. The behavior of the derived solutions is examined for the cases of a monodisperse and three polydisperse colloid distributions. Based on data gathered from reported field studies, a log-normal distribution of colloid sizes was used for the polydisperse plumes. A comparison of the analytical solution for instantaneous colloid injection into a fracture with no reaction at the walls and experimental data for coliphages traveling down a 19 cm natural fracture is made. Using a non-linear least squares estimate for the fracture cross-sectional area, excellent agreement between the experimental data and the analytical breakthrough curve was observed.

Acknowledgements

S.C.J. is grateful for the support provided by the University of California, Irvine through the Regents' Fellowship. S.C.J. would also like to acknowledge John Pezzullo of Georgetown University for many stimulating discussions. Many thanks to Brian Berkowitz of the Weizmann Institute of Science, Rheovat, Israel whose thoughtful and detailed review substantially improved this manuscript. Sandia is a multiprogram laboratory operated by Sandia Corporation, a Lockheed Martin Company for the United States Department of Energy's National Nuclear Security Administration under contract DE-AC04-94AL85000.

Appendix A. Nomenclature

b	fracture aperture (L)
d_p	colloid diameter (L)
D_{eff}	effective dispersion coefficient for a plume of finitely sized colloids (L^2t^{-1})
D_{Taylor}	Taylor dispersion coefficient for a plume of infinitesimally small colloids (solute) (L^2t^{-1})
$\mathcal{D}_{d_p}$	molecular diffusion coefficient of a colloid with diameter d_p (L^2t^{-1})
Da	Damköhler number, defined as $k_f b/\mathcal{D}_{d_p}$
k	Boltzmann's constant ($ML^2t^{-2}T^{-1}$)
k_f	forward filtration rate constant (Lt^{-1})
k_r	surface distribution coefficient (for reversible filtration) (L)
K_{eff}	effective decay coefficient (t^{-1})
n	number concentration of monodisperse colloids per unit volume of interstitial fluid (L^{-3})
n_{d_p}	number concentration of a polydisperse concentration of a colloid distribution per unit volume of interstitial fluid (L^{-3})
n_o	initial number concentration of monodisperse colloids (L^{-2} or L^{-3})
$n_{o_{d_p}}$	initial number concentration of a polydisperse colloid distribution (L^{-2} or L^{-3})
n_{pdf}	probability density function of polydisperse colloids (L^{-3} or L^{-4})
$\bar{n}$	average number concentration of monodisperse colloids across a fracture per unit volume of interstitial fluid (L^{-3})
$\bar{n}_{d_p}$	average number concentration of a polydisperse colloid distribution across a fracture per unit volume of interstitial fluid (L^{-3})
$n^*_{d_p}$	number of attached colloids per unit surface area of the fracture wall (L^{-2})
$N_o(d_p)$	initial number sub-concentration of colloids with diameter d_p in the polydisperse distribution introduced into a fracture (L^{-2} or L^{-3})
R	retardation factor
t	time (t)
T	absolute temperature of the interstitial fluid (T)
$u(z)$	local interstitial fluid velocity (Lt^{-1})
$\bar{U}$	mean interstitial fluid velocity (Lt^{-1})
U_{eff}	effective velocity of a colloid plume (Lt^{-1})
U_{max}	maximum interstitial fluid velocity at the facture centerline in the x-direction (Lt^{-1})

x	coordinate along the fracture length parallel to the fracture aperture (L)
z	coordinate perpendicular to the fracture (L)

Greek letters

δ	Dirac delta function (L^{-1})
ζ^2	variance of the log-diameters for a polydisperse distribution of colloids
η	dynamic viscosity of the interstitial fluid ($ML^{-1}t^{-1}$)
λ	mean of the log-diameters for a polydisperse distribution of colloids
μ	arithmetic mean of the diameters for a colloid plume (L)
ξ	coordinate transformation, equal to $x-U_{eff}t$ (L)
σ	standard deviation of the diameters for a colloid plume (L)
Ω	velocity coefficient for constant concentration inlet colloid transport subject to irreversible attachment (Lt^{-1})

References

[1] A. Abdel-Salam, C.V. Chrysikopoulos, Analysis of a model for contaminant transport in fractured media in the presence of colloids, J. Hydrol. 165 (1995) 261–281.

[2] A. Abdel-Salam, C.V. Chrysikopoulos, Modeling of colloid and colloid-facilitated contaminant transport in a two-dimensional fracture with spatially variable aperture, Transport Porous Med. 20 (3) (1995) 197–221.

[3] M. Ibaraki, E.A. Sudicky, Colloid-facilitated contaminant transport in discretely fractured porous media 1. Numerical formulation and sensitivity analysis, Water Resour. Res. 31 (12) (1995) 2945–2960.

[4] J.H. Kessler, J.R. Hunt, Dissolved and colloidal contaminant transport in a partially clogged fracture, Water Resour. Res. 30 (4) (1994) 1195–1206.

[5] R. Johnson, S. Ning, M. Elimelech, Colloid transport in geochemically heterogeneous porous media: Modeling and measurements, Env. Sci. Technol. 30 (1996) 3284–3293.

[6] C.V. Chrysikopoulos, A. Abdel-Salam, Modeling colloid transport and deposition in saturated fractures, Colloids Surf. A Physicochem. Eng. Aspects 121 (1997) 189–202.

[7] J.F. McCarthy, J.M. Zachara, Subsurface transport of contaminants, Env. Sci. Technol. 23 (1989) 5.

[8] J.F. McCarthy, C. Degueldre, Environmental Particles, Lewis, Boca Raton, Florida, 1993 (Chapter 2).

[9] A.B. Kersting, D.W. Efurd, D.L. Fnnegan, D.J. Rokop, D.K. Smith, J.L. Thompson, Migration of plutonium in groundwater at the nevada test site, Nature 397 (1999) 56–59.

[10] P. Vilks, M.-H. Baik, Laboratory migration experiments with radionuclides and natural colloids in a granite fracture, J. Contam. Hydrol. 47 (2001) 197–210.

[11] R.W. Buddemeier, J.R. Hunt, Transport of colloidal contaminants in groundwater radionuclide migration at the nevada test site, Appl. Geochem. 3 (1988) 535–548.

[12] J.I. Drever, The Chemistry of Weathering, Reidel, Dordrecht, 1985.

[13] C.V. Chrysikopoulos, Transport of colloids in saturated fractures, in: Advances in Fracture Mechanics: Fractured Rock, Computational Mechanics Publications, WIT Press, 1999, pp. 297–330 (Chapter 10).

[14] G.I. Taylor, Dispersion of soluble matter in solvent flowing slowly through a tube, Proc. R. Soc. London A 219 (1953) 186–203.

[15] R. Aris, On the dispersion of a solute in a fluid flowing through a tube, Proc. R. Soc. London A 235 (1956) 67–77.

[16] R. Sankarasubramanian, W.N. Gill, Unsteady convective diffusion with interphase mass transfer, Proc. R. Soc. London A 333 (1974) 115–132.

[17] H. Brenner, A general theory of taylor dispersion phenomena, Physicochem. Hydrodynam. 1 (1980) 91–123.

[18] H. Brenner, A general theory of taylor dispersion phenomena II: An extension, Physicochem. Hydrodynam. 3 (1982) 133–157.

[19] A.E. DeGance, L.E. Johns, On the dispersion coefficients for Poiseuille flow in a circular cylinder, Appl. Sci. Res. 34 (1978) 227–258.

[20] M. Shapiro, H. Brenner, Taylor dispersion of chemically reactive species: lrreversible first-order reactions in bulk and on boundaries, Chem. Eng. Sci. 41 (6) (1986) 1417–1433.

[21] M. Shapiro, H. Brenner, Chemically reactive generalized Taylor dispersion phenomena, AIChE J. 33 (7) (1987) 1155–1167.

[22] M. Shapiro, H. Brenner, Dispersion of a chemically reactive solute in a spatially periodic model of a porous medium, Chem. Eng. Sci. 43 (3) (1988) 551–571.

[23] D.H. Tang, E.O. Frind, E.A. Sudicky, Contaminant transport in fractured porous media: Analytical solution for a single fracture, Water Resour. Res. 17 (3) (1981) 555–564.

[24] E.A. Sudicky, E.O. Frind, Contaminant transport in fractured media: Analytical solutions for a system of parallel fractures, Water Resour. Res. 18 (6) (1982) 1634–1642.

[25] J. Cormenzana, Transport of a two-member decay chain in a single fracture: Simplified analytical solution for two radionuclides with the same transport properties, Water Resour. Res. 36 (5) (2000) 1339–1346.

[26] A. Abdel-Salam, C.V. Chrysikopoulos, Analytical solutions for one-dimensional colloid transport in saturated fractures, Adv. Water Resour. 17 (1994) 283–296.

[27] S.C. James, C.V. Chrysikopoulos, Effective velocity and effective dispersion coefficient for finitely sized particles flowing in a uniform fracture, J. Coll. Interf. Sci. 263 (1) (2003) 288–295.

[28] S.C. James, C.V. Chrysikopoulos, Transport of polydisperse colloid suspensions in a single fracture, Water Resour. Res. 35 (3) (1999) 707–718.
[29] S.C. James, C.V. Chrysikopoulos, Transport of polydisperse colloids in a saturated fracture with spatially variable aperture, Water Resour. Res. 36 (6) (2000) 1457–1465.
[30] C.V. Chrysikopoulos, S.C. James, Transport of neutrally buoyant and dense variably sized colloids in a two-dimensional fracture with anisotropic aperture, Transport Porous Med. 51 (2003) 191–210.
[31] R.W. Fox, A.T. McDonald, Introduction to Fluid Mechanics, fifth ed., Wiley, New York, NY, 1998.
[32] M.K. Lyon, L.G. Leal, An experimental study of the motion of concentrated suspensions in two-dimensional channel flow. Part 1. Monodisperse systems, J. Fluid Mech. 363 (1998) 25–56.
[33] M.K. Lyon, L.G. Leal, An experimental study of the motion of Concentrated suspensions in two-dimensional channel flow. Part 1. Bidisperse systems, J. Fluid Mech. 363 (1998) 57–77.
[34] R.B. Bird, W.E. Stewart, E.N. Lightfoot, Transport Phenomena, Wiley, 1960.
[35] M. Han, H. Lee, Collision efficiency factor in brownian coagulation α_{Br}: Calculation and experimental verification, Colloids Surf. A Physicochem. Eng. Aspects 202 (2002) 23–31.
[36] D.A. Edwards, M. Shapiro, I.I. Brenner, M. Shapira, Dispersion of inert solutes in spatially periodic two dimensional model porous media, Transport Porous Med. 6 (1991) 337–358.
[37] A.A. Keller, P.V. Roberts, P.K. Kitanidis, Prediction of single phase transport parameters in a variable aperture fracture, Geophys. Res. Lett. 22 (11) (1995) 1425–1428.
[38] S.C. James, C.V. Chrysikopoulos, An efficient particle tracking equation with a specified spatial step for the solution of the diffusion equation, Chem. Eng. Sci. 56 (23) (2001) 6535–6543.
[39] L.E. Johns, A.E. DeGance, Dispersion approximations to the multicomponent convective, diffusion equation for chemically active systems, Chem. Eng. Sci. 30 (1975) 1065–1067.
[40] B. Berkowitz, J. Zhou, Reactive solute transport in a single fracture, Water Resour. Res. 32 (4) (1996) 901–913.
[41] P. Dijk, B. Berkowitz, Precipitation and dissolution of reactive solutes in fractures, Water Resour. Res. 34 (3) (1998) 457–470.
[42] J.B. Butt, Reaction Kinetics and Reactor Design, Prentice Hall, 1980.
[43] H.S. Carslaw, J.C. Jaeger, Conduction of Heat in Solids, second ed., University Press, Oxford, 1988.
[44] W.N. Gill, R. Sankarasubramanian, Dispersion of non-uniformly distributed time–variable continuous sources in time-dependent flow, Proc. R Soc. London A 327 (1972) 191–208.
[45] R. Sankarasubramanian, W.N. Gill, Dispersion from a prescribed concentration distribution in a time variable flow, Proc. R. Soc. London A 329 (1972) 479–792.
[46] Z. Adamczyk, B. Siwek, M. Zembala, Reversible and irreversible adsorption of particles on homogeneous surfaces, Colloids Surf. A Physicochem. Eng. Aspects 62 (1992) 119–130.
[47] M. Shapiro, A. Oron, C. Gutfinger, A dispersion model for electrostatic precipitation of particles from turbulent flows, Physicochem. Hydrodynam. 10 (4) (1988) 471–491.
[48] P.A. Domenico, F.W. Schwartz, Physical and Chemical Hydrogeology, Wiley, New York, NY, 1990.
[49] M.T. van Genuchten, W.J. Alves, Analytical solutions of the one dimensional convective dispersive solute transport equations. Technical Bulletin 1661, U.S. Department of Agriculture (1982).
[50] B.S. Lartiges, S. Deneux-Mustin, G. Villemin, C. Mustin, O. Baxrès, M. Chamerois, B. Gerard, M. Babut, Composition, structure and size distribution of suspended particulates from the Rhine river, Water Res. 35 (3) (2001) 808–816.
[51] P. Rossé, J.-L. Loizeau, Use of single particle counters for the determination of the number and size distribution of colloids in natural surface waters, Colloids Surf. A Physicochem. Eng. Aspects 217 (2002) 109–120.
[52] A. Ledin, S. Karlsson, A. Düker, B. Allard, Measurements *in situ* of concentration and size distribution of colloidal matter in deep groundwater by photon correlation spectroscopy, Water Res. 28 (7) (1994) 1539–1545.
[53] A.H.-S. Ang, W.H. Tang, Probability Concepts in Engineering Planning and Design, Wiley, 1975.
[54] P. Warszynski, Coupling of hydrodynamic and electric interactions in absorption of colloidal particles, Adv. Colloid Interf. Sci. 84 (2000) 47–142.
[55] P.W. Reimus, The use of synthetic colloids in tracer transport experiments in saturated rock fractures. Ph.D. thesis, Los Alamos National Laboratory, LA 13004-T 1995.
[56] R.C. Bales, C.P. Gerba, G. Grondin II, S.L. Jensen, Bacteriophage transport in a sandy soil and fractured tuff, Appl. Env. Microbio. 55 (8) (1989) 2061–2067.
[57] J.C. Pezzullo, Available from http://members.aol.com/johnp71/nonlin.html (2000).